PHYSICAL REVIEW B **88**, 245112 (2013)

ARPES study of the effect of Cu substitution on the electronic structure of NaFeAs

S. T. Cui,[1] S. Kong,[1] S. L. Ju,[1] P. Wu,[1] A. F. Wang,[2] X. G. Luo,[2] X. H. Chen,[2] G. B. Zhang,[1] and Z. Sun[1,*]

[1]*National Synchrotron Radiation Laboratory, University of Science and Technology of China, Hefei, Anhui 230029, People's Republic of China*

[2]*Hefei National Laboratory for Physical Sciences at Microscale and Department of Physics, University of Science and Technology of China, Hefei, Anhui 230026, People's Republic of China*

(Received 21 October 2013; revised manuscript received 22 November 2013; published 10 December 2013)

Using high-resolution angle-resolved photoemission spectroscopy, we studied the electronic structure of $NaFe_{1-x}Cu_xAs$ ($x = 0.019, 0.045, 0.14$). With increasing the doping concentration, we found that the Cu dopant introduces extra charge carriers. The overall band dispersions barely change with doping, suggesting that the Cu substitution does not affect local correlations. Similar to the case of $NaFe_{1-x}Co_xAs$, one electron pocket emerges at the Brillouin zone center at high doping levels. Moreover, the near-E_F spectral weight decreases with increasing the Cu dopant, which explains why the $NaFe_{1-x}Cu_xAs$ shows a poor electronical conductivity at high doping levels.

DOI: 10.1103/PhysRevB.88.245112 PACS number(s): 74.25.Jb, 71.20.−b, 74.70.Xa, 79.60.−i

In the studies of iron-pnictide superconductors, chemical substitutions have been widely employed to tune the fundamental electronic structures and macroscopic physical properties. For instance, they can suppress the structural and magnetic transitions and induce superconductivity,[1–7] change local electronic and magnetic correlations,[7–9] control the concentration of electron or hole carriers and shift the Fermi level,[10,11] and serve as impurities.[12–15] Accordingly, the effects of chemical substitutions have provided numerous clues on the underlying interactions and pairing mechanism in iron-pnictides.

In the so-called 122 family, from the perspective of band structures, the primary role of Co substitution is to dope one extra electron per Co atom, which results in a shift of Fermi energy and a variation of the Fermi surface nesting between electron and hole pockets.[10,11] Such a change of the band structures is believed to be responsible for the emergence of superconductivity. Similar to the case of Co substitution, Ni provides two extra electrons per atom and results in a phase diagram resembling the Co-doped system if we count extra electrons per Fe site doped by Co or Ni.[4,16,17] Following this trend, one may expect Cu dopes three electrons per atom and induces superconductivity. However, this is not the case, though the magnetic and structural transitions are suppressed in a fashion similar to that of Co and Ni doped samples.[4,17] In $Ba(Fe_{1-x}Cu_x)_2As_2$, superconductivity emerges within a very narrow doping range and with $T_c < 3$ K.[16] Similar behavior has also been observed in $Sr(Fe_{1-x}Cu_x)_2As_2$, where no superconductivity was found.[18]

Controversial results have been reported on the physics of Cu substitution in 122 families. Some measurements indicate that Cu can slightly dope extra electron carriers with strong impurity potential,[19,20] but it has also been suggested that Cu in FeAs layers may have a $3d^{10}$ configuration and gives rise to a hole doping of Fe bands.[18,21,22] To gain more knowledge about the effect of Cu doping, it is important to extend investigations to other families of FeAs compounds, for instance the 111 type. In iron-pnictides, the FeAs layer is the key element that determines the main physics. When Cu is doped in 111 families, one may expect that superconductivity is strongly suppressed, since the Cu substitution for Fe does not favor superconductivity in 122 families. NaFeAs is a filamentary superconductor without bulk superconductivity.[23] Contrary to the case in 122 family, a very slight Cu substitution in NaFeAs can induce bulk superconductivity.[24] The superconductivity was observed in $NaFe_{1-x}Cu_xAs$ in a relatively large doping range ($x = 0$–0.045) with T_c as high as 11.5 K. These properties are in sharp contrast with the case in 122 families. This marked difference between 111 and 122 families raises questions about the role of Cu substitution in NaFeAs and potentially may reveal some clues on the underlying physics on the pairing mechanism in iron-pnictides.

$NaFe_{1-x}Cu_xAs$ is an ideal system for angle-resolved photoemission spectroscopy (ARPES) to investigate the electronic structure of iron-pnictide materials, because there is no surface reconstruction or charge redistribution. To obtain insights into the nature of the puzzling properties of Cu-doped FeAs-based materials, we performed a systematic ARPES measurement on the Cu-substituted 111-type NaFeAs single crystals. We focused on the band dispersions and the shifting of the Fermi energy as a function of Cu doping from $x = 0.019$, $x = 0.045$ to $x = 0.14$ above the structural, spin-density wave (SDW), and superconducting transition temperatures. Thus, the primary change in electronic properties should be induced by the Cu dopant, while the influences of the structural and magnetic transitions are eliminated. We found that similar to the case of Co-doped NaFeAs, the Fermi level of $NaFe_{1-x}Cu_xAs$ increases with the Cu dopant, which implies an electron doping behavior. The overall band dispersions remain almost the same from $x = 0.019$ sample to $x = 0.045$ and $x = 0.14$ samples. Moreover, we found that the near-E_F spectral weight is strongly suppressed in $x = 0.14$ compound, consistent with the general doping dependence of resistivity in these materials.

High-quality single crystals of $NaFe_{1-x}Cu_xAs$ were synthesized using flux method as described in[24] with NaAs as the flux. The chemical compositions of the single crystals were determined by energy-dispersive x-ray spectroscopy with a standard instrument error ∼10%. ARPES studies were performed at the SIS beamline of the Swiss Light

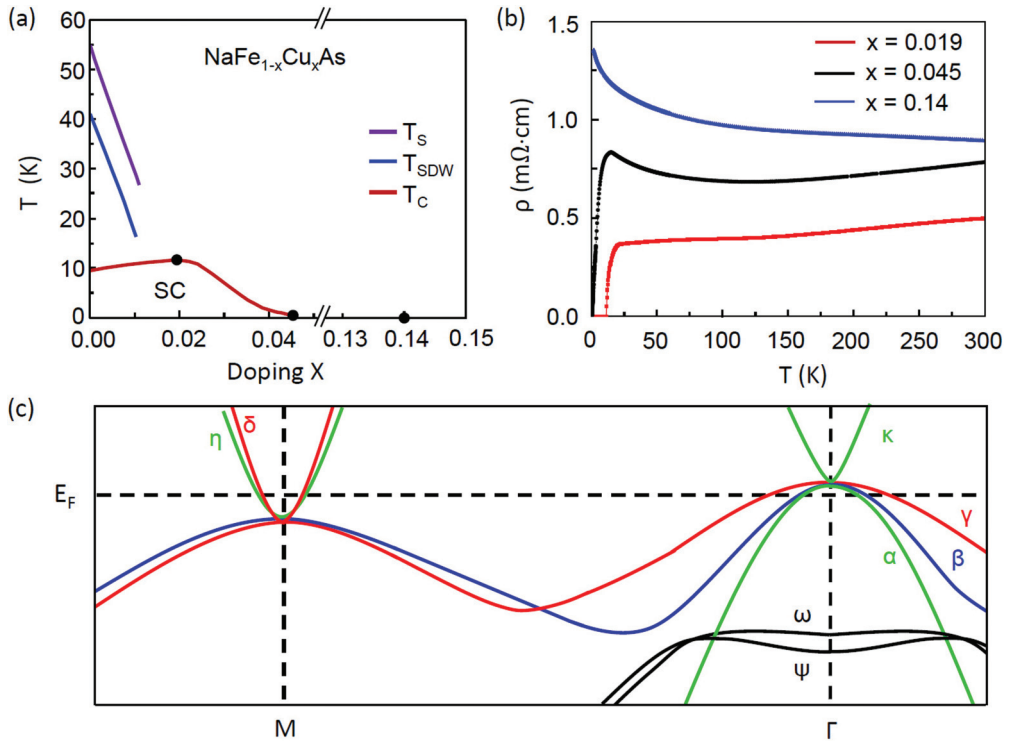

FIG. 1. (Color online) (a) Phase diagram of $NaFe_{1-x}Cu_xAs$. The structural (T_S), spin-density-wave (T_{SDW}) and superconducting (T_c) transitions were determined by transport measurements in Ref. 24. The black dots mark the T_c's and compositions of the three compounds we studied. (b) In-plane resistivities of $NaFe_{1-x}Cu_xAs$ for $x = 0.019$, $x = 0.045$, and $x = 0.14$ compounds. (c) A schematic band structure of NaFeAs. As will be shown, the Fermi energy moves up with the increasing of Cu substitution and a small electron pocket around the zone center Γ will emerge in the heavily overdoped regime.

Source (SLS), using a Scienta R4000 electron spectrometer. The angular resolution was 0.3 degrees and the combined instrumental energy resolution was better than 20 meV. All samples were cleaved *in situ* and measured at 25 K under a vacuum better than 5×10^{-11} mbar.

The electronic phase diagram of $NaFe_{1-x}Cu_xAs$ is plotted in Fig. 1(a), which was determined by transport measurements from the same sample batches.[24] The black dots indicate the compositions and T_c's of three compounds ($x = 0.019$,0.045, and 0.14) we studied here, and their in-plane resistivities are shown in Fig. 1(b). The T_S and T_{SDW} were determined by various transport measurements as shown in Ref. 24, which shows no sign of structural or SDW transitions in the compounds we presented in this paper. Moreover, we performed experiments at $T = 25$ K to avoid the undetected structural or SDW transitions. The $x = 0.019$ compound is the optimally doped composition with $T_c \sim 11.5$ K, the $x = 0.045$ is in the overdoped regime with superconductivity at very low temperature and is close to the boundary of the superconducting dome, and for the heavily overdoped $x = 0.14$ compound, the in-plane resistivity data suggests a semiconducting behavior. Figure 1(c) shows a schematic plot of the band structure of NaFeAs along the Γ-M direction, which is helpful to identify individual bands in the ARPES data.

In Fig. 2, we show the Fermi surface mappings of $NaFe_{1-x}Cu_xAs$ for $x = 0.019$, $x = 0.045$, and $x = 0.14$ compounds. All data were measured at $T = 25$ K to reveal systematic variations of band structures as a function of doping. Both *p*- and *s*-polarized photons were used for the measurements, and the polarizations are indicated in individual panels. Since the electronic states near the Fermi energy are primarily composed of the d_{xz}, d_{yz}, and d_{xy} orbitals, the photoemission matrix elements can be drastically different for *p*- and *s*-polarized photons. Thus, the intensity distributions for the Fermi surface mappings vary significantly from *p* to *s* polarizations, as shown in Fig. 2. These results are consistent with the investigation of NaFeAs previously reported by Zhang *et al.*[25] From $x = 0.019$, $x = 0.045$ to $x = 0.14$, the electron pockets around M_x or M_y points gradually increase in size with the Cu dopants. This behavior suggests that the Cu substitution in NaFeAs indeed dopes extra electron carriers, similar to the case in $Ba(Fe_{1-x}Cu_x)_2As_2$.[19]

In order to illustrate more details on the effects of Cu substitution on electronic structures of the NaFeAs system, we compared band dispersions along high symmetry lines. Figures 3(a_1)–3(c_1) show photoemission intensity plots along the orange cuts in Figs. 2(a_1)–2(c_1), and the corresponding second-derivative images are shown in Figs. 3(a_2)–3(c_2) to manifest the band dispersions. Because these data were taken using *p*-polarized photons, detailed calculations suggest that d_{xz} orbital states will show up and d_{yz} orbital states should be strongly suppressed.[25] Here we denote the band in Fig. 3(a_1) as α. With the increasing of Cu dopant, a small electron pocket, κ, emerges in $x = 0.045$ and $x = 0.14$ compounds, which is similar to the band structure in heavily overdoped $NaFe_{1-x}Co_xAs$.[26] Such a small electron pocket is consistent

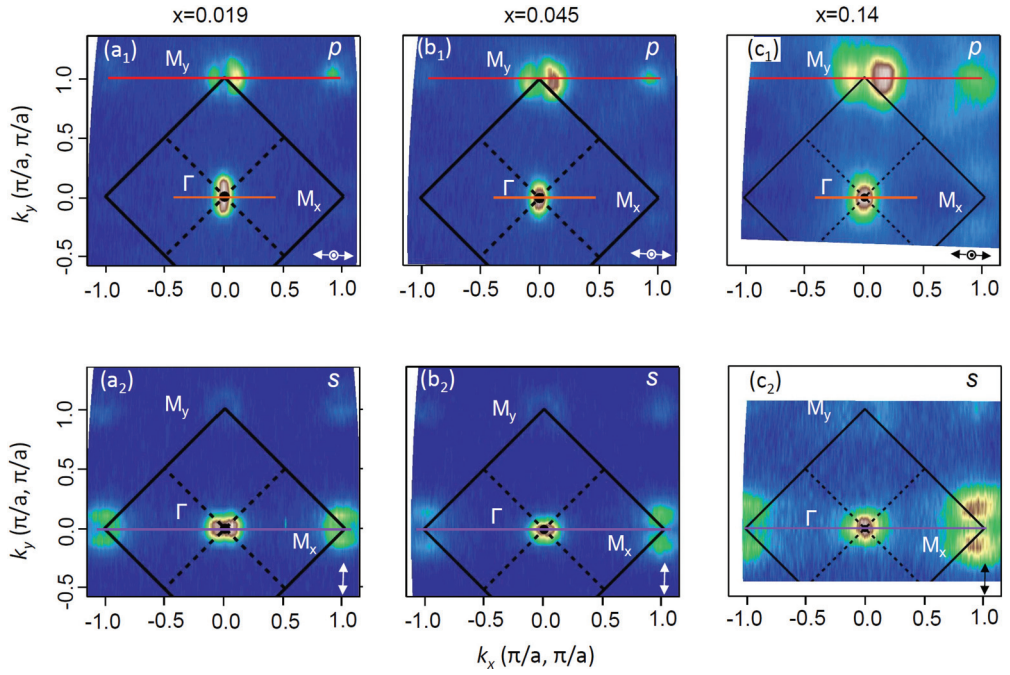

FIG. 2. (Color online) The photoemission intensity maps of $NaFe_{1-x}Cu_xAs$ at the Fermi levels for (a) $x = 0.019$, (b) $x = 0.045$, and (c) $x = 0.14$ compounds, with primary p (top row) and s (bottom row) geometries. All intensity maps were obtained by integrating spectral weight over an energy window of $E_F \pm 5$ meV. The black squares mark the first Brillouin zones. k_x and k_y are along the directions of nearest neighboring Fe-Fe bonds. All data were taken at 25 K using 85 eV photons.

with first-principles calculations that show an electronlike band sitting above the holelike bands at the zone center.[27,28] Similar electron pockets have also been observed in other heavily electron-doped iron-pnictides.[11,26,29]

Taken using s-polarized photons, Figs. 3(d_1)–3(f_1) display photoemission intensity plots along the purple cuts in Figs. 2(a_2)–2(c_2). According to the calculations of photoemission matrix element,[25] electronic states of d_{xz} orbital can be heavily suppressed and d_{yz} states should appear instead. Therefore, the strong dispersive spectral weight, denoted as β, consists primarily of d_{yz} orbital states, which is strikingly different from the bands observed in Figs. 3(a_1)–3(c_1). The band dispersions for various dopings can be illustrated in the second-derivative images as shown in Figs. 3(d_2)–3(f_2). We note that the γ band [see Fig. 1(c)] cannot be clearly resolved around the zone center, because the d_{xy} orbital symmetry of this band makes the spectral weight strongly suppressed for both p- and s-polarized photons.[25,26]

The E vs k dispersions of the α, β, and κ bands for various dopings can be determined on the basis of the second-derivative images in Figs. 3(a_2)–3(c_2) and 3(d_2)–3(f_2). In Fig. 3(g), all these dispersions for various doping levels are plotted and overlay each other by shifting them in energy, with their Fermi levels indicated respectively. Though the $NaFe_{1-x}Cu_xAs$ compound changes from an optimally doped superconductor ($x = 0.019$) to a heavily overdoped semiconductor ($x = 0.14$), it is evident that the band dispersions for various doping levels remain almost the same over a large energy scale of ~100 meV except a rigid shifting in energy. In Fig. 3(g), the Fermi level shifts about 7 ± 4 meV and 20 ± 4 meV, respectively, from $x = 0.019$ sample to $x = 0.045$ and $x = 0.14$ samples.

We have also examined how the band structures around the zone corners change as a function of Cu doping. Along the red lines in Figs. 2(a_1-c_1), we took photoemission spectra and shown them in Figs. 4(a_1-c_1). Their second-derivative images are shown in Figs. 4(a_2-c_2). The electronic structure calculations[27] and ARPES measurements on NaFeAs[25,30] indicate that there are two electronlike bands around the M point with different orbital symmetries. Here, only one band (denoted as η,δ) can be resolved around the zone corner M_y (see Fig. 2). It is likely either because one of them is suppressed by the photoemission matrix elements or they are nearly degenerate and cannot be clearly distinguished in our experiments. This electron pocket slightly moves to deeper binding energies with the increasing of Cu dopant. In addition, there is strong dispersive spectral weight around −200 meV, which should be attributed to the ω and ψ bands as shown in Fig. 1(c). In Fig. 4(d), we plot all band dispersions determined by the second-derivative images. By shifting these dispersions in energy, we can align them with each other with excellent agreement and estimate the shifting value of the Fermi levels with increasing Cu dopant. Compared to the $x = 0.019$ compound, the Fermi level moves up about 7 ± 4 meV and 20 ± 4 meV in $x = 0.045$ and $x = 0.14$ compounds, respectively, which is in excellent agreement with the values we found in Fig. 3.

In NaFeAs, the k_z dispersion is relatively weak,[27] so we can estimate the carrier concentrations on the basis of the Fermi surfaces and Fermi crossings. Approximately, the extra electron carriers doped by Cu are 0.07, 0.1, and 0.18 per unit cell for $x = 0.019$,0.045, and 0.14 compounds, respectively. Averagely, each Cu atom dopes about 1.9, 1.1, and 0.64 extra electrons for $x = 0.019$,0.045, and 0.14 compounds,

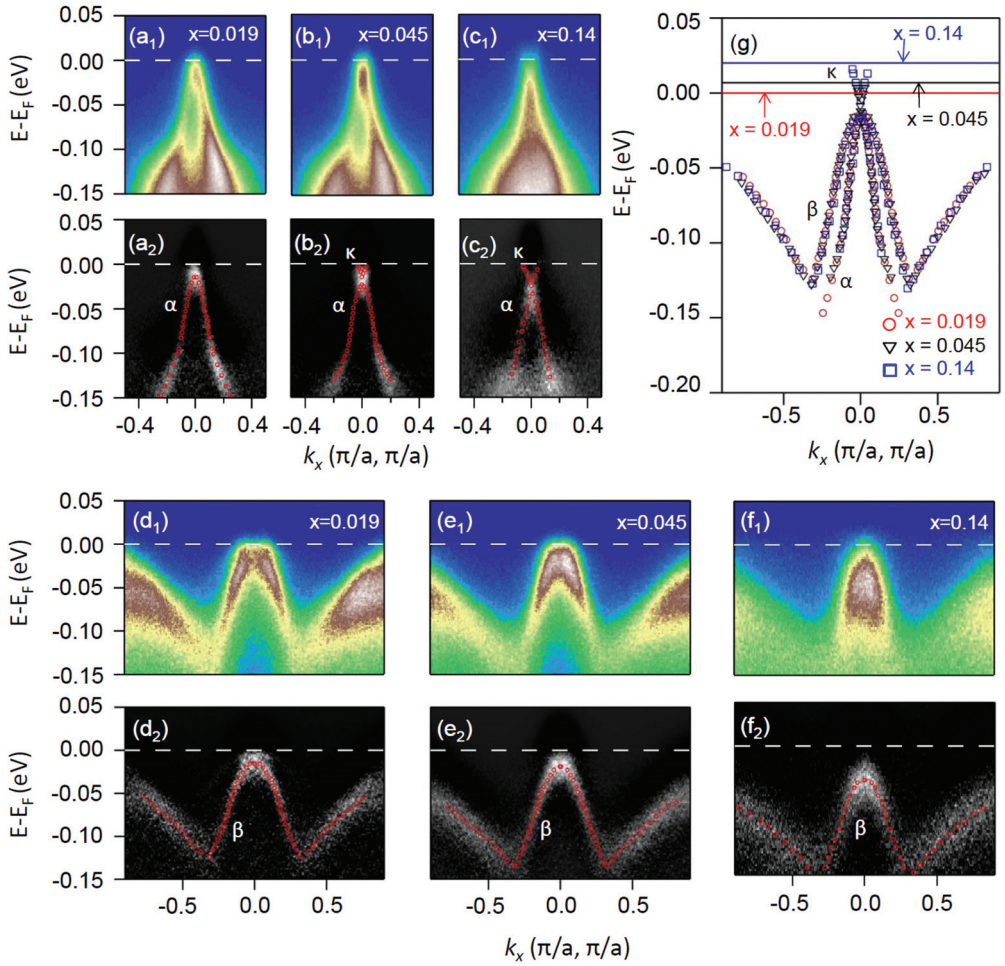

FIG. 3. (Color online) (a_1)–(c_1) The photoemission plots along the Γ-M direction [orange lines in Figs. 2(a_1)–2(c_1)] taken with p-polarized photons for $x = 0.019$, $x = 0.045$, and $x = 0.14$ compounds, respectively. (a_2)–(c_2) The second-derivative images of panels (a_1)–(c_1). (d_1)–(f_1) The photoemission plots along the Γ-M direction [purple lines in Figs. 2(a_2)–2(c_2)] taken with s-polarized photons for $x = 0.019$, $x = 0.045$, and $x = 0.14$ compounds, respectively. (d_2)–(f_2) The second-derivative images of panels (d_1)–(f_1). The band dispersions revealed by the second-derivative images are indicated by red circles. (g) A summary of the band dispersions along the Γ-M direction for $x = 0.019$, $x = 0.045$, and $x = 0.14$ compounds, with their Fermi levels indicated individually.

respectively, though for a rigid-band model each Cu atom is expected to release three electrons. This behavior suggests that the Cu dopant can provide more extra electrons at low doping than at high doping levels, which is very different from the case in Cu-doped $BaFe_2As_2$. In $Ba(Fe_{1-x}Cu_x)_2As_2$, as illustrated by Ideta *et al.*, in the range of $x = 0.04$–0.14, each Cu atom contributes one extra electron, approximately.[19] In fact, as will be shown in Fig. 5, the overall near-E_F electronic states reduce with increasing Cu dopant in $Na(Fe_{1-x}Cu_x)As$, which implies that at high doping levels the effective carrier doping is much less than the numbers as calculated above on the basis of the Fermi surface topology.

Figures 3(g) and 4(d) suggest that the Cu substitution results in a rigid-band-like shifting of band structures. However, similar to the situation in Cu-doped $BaFe_2As_2$,[19] the electron counting indicates that the Cu substitution provides less extra electrons than expected from a perspective of the rigid-band model. Moreover, as will be shown in Fig. 5(a), the Cu substitution induces strong impurity potential. Generally speaking, the overall band dispersions in iron-pnictides are renormalized by local interactions, including the Hubbard U and Hund's coupling J. The behavior of rigid-band-like shifting in band structures suggests that Cu dopant has no effect on the local interactions of U and J.

Figure 5(a) shows the angle-integrated photoemission spectra. An evident feature around −4 eV grows up with the Cu substitution. This feature should be attributed to localized Cu $3d$ states, as suggested by both theoretical calculations and ARPES measurements on Cu-doped $BaFe_2As_2$.[12,19] Figures 5(b) and 5(c) show angle-integrated spectral weight in Figs. 3(a_1)–3(c_1) and Figs. 4(a_1)–4(c_1) over a momentum window $(-0.5$–$0.5)$ $(\pi/a, \pi/a)$, respectively. One can notice that the near-E_F spectral weight gradually decreases with the increasing of Cu dopant. This reduction of spectral weight near the Fermi level is consistent with the increase of normal-state resistivity [see Fig. 1(b)] as a function of Cu concentration. In addition, the impurity effect induced by Cu dopant can play additional role, which should be responsible for the semiconducting or insulating behavior of the $x = 0.14$ compound shown in Fig. 1(b), despite the fact that

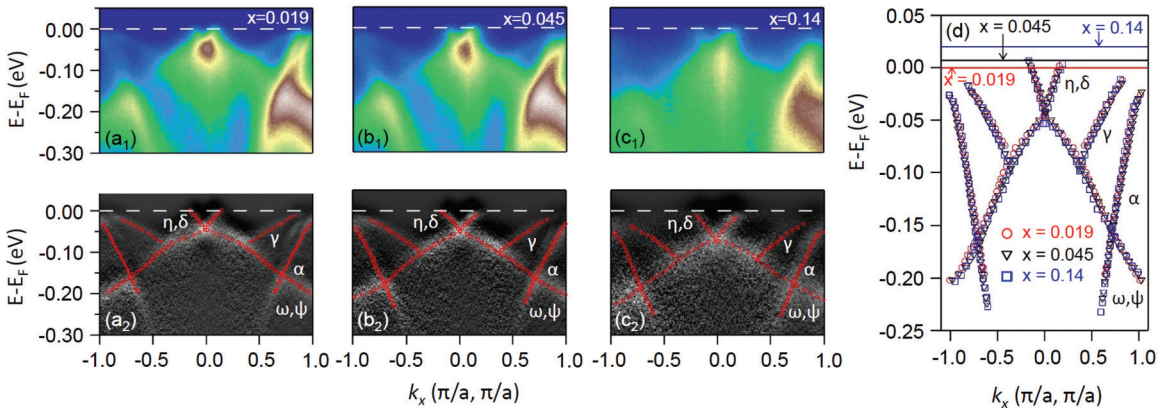

FIG. 4. (Color online) (a_1)–(c_1) The photoemission plots along the red lines in Figs. 2(a_1)–2(c_1) for $x = 0.019$, $x = 0.045$, and $x = 0.14$ compounds, respectively. (a_2)–(c_2) The corresponding second-derivative images. The red circles indicate the band dispersions revealed by the second-derivative images. (d) A summary of the band dispersions along the red lines in Figs. 2(a_1)–2(c_1), with their Fermi levels indicated respectively.

the emergence of the κ band and the increase of Fermi velocity in the zone-corner electron pockets can facilitate the electron conduction. Theoretical studies suggest that the reduction of the near-E_F spectral weight is caused by the increase of the impurity band splitting from the host band.[12,31,32] As suggested by the semiconducting behavior of resistivity of $x = 0.14$, the near-E_F spectral weight will further decrease as the temperature goes down. Here, we can illustrate the effect of Cu substitution on the density of states of NaFeAs system in Fig. 5(d)—though some 3d states of Cu dopant are localized

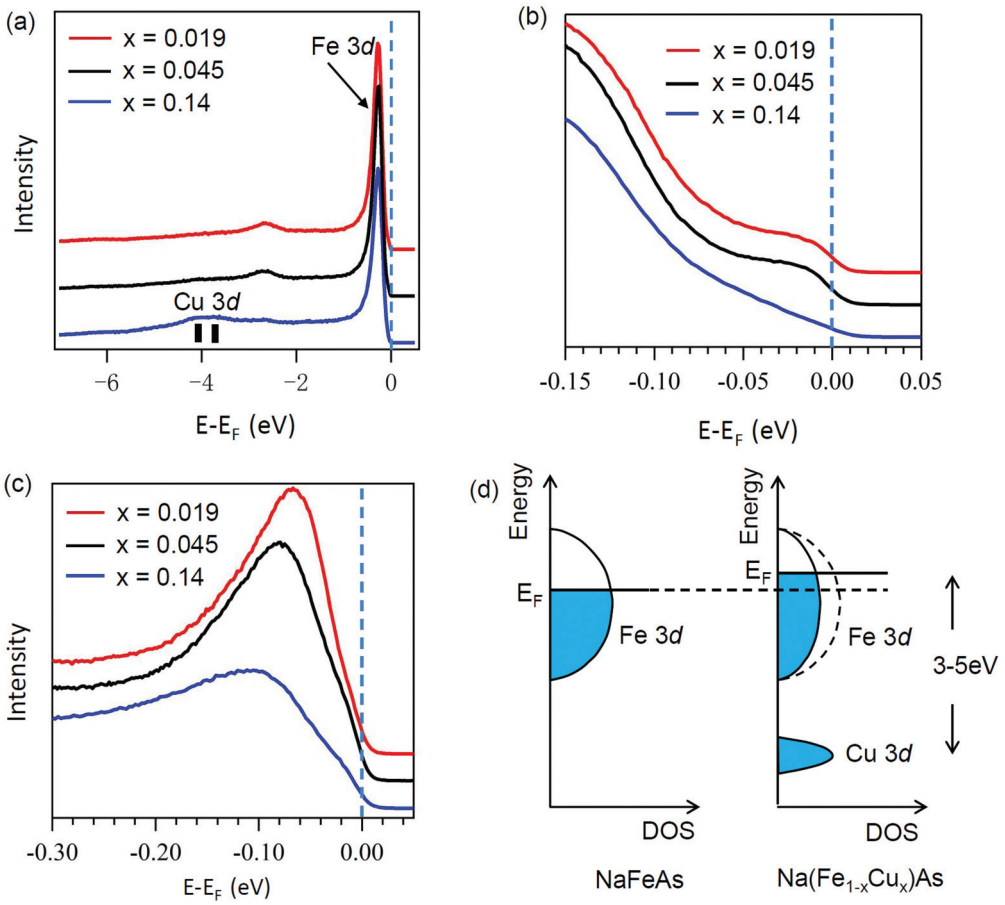

FIG. 5. (Color online) (a) Angle-integrated photoemission intensity of $NaFe_{1-x}Cu_xAs$. The shadow area shows the spectral weight dominated by Cu 3d-derived states. (b), (c) The angle-integrated spectral weight in Figs. 2(a_1)–2(c_1) and Figs. 3(a_1)–3(c_1) over a momentum window (-0.5–0.5) ($\pi/a, \pi/a$), respectively. (d) A schematic plot of the density of states for NaFeAs and $NaFe_{1-x}Cu_xAs$.

about −4 eV below the Fermi level, it also provides some 3*d* electrons to the itinerant Fe 3*d* states and increases the Fermi energy, meanwhile the near-E_F density of states reduces.

From the optimally doped superconducting compound ($x = 0.019$) to the semiconducting one ($x = 0.14$), the vanishing of superconductivity accompanies the changes of electronic structures. As shown in our data, the most drastic change in the band structures is the emergence of the κ electron pocket at the zone center. Indeed, such a change of band structures has also been observed in overdoped $NaFe_{1-x}Co_xAs$ and $Ba(Fe_{1-x}Co_x)_2As_2$, where a similar correlation between the appearance of the central electron pocket and the disappearance of the superconductivity has been found.[10,26] These studies suggest that the underlying Fermi surface topology is very important for the persistence of superconductivity in the overdoped region, and that the critical doping levels for superconductivity is in the vicinity of Lifshitz transitions.[10,11,33] On the other hand, the decrease of near-E_F density of states and the increase of Cu impurities[12] can contribute additional effects to suppress the superconductivity in the overdoped region.

In summary, we have studied the band structures of $NaFe_{1-x}Cu_xAs$ ($x = 0.019, 0.045, 0.14$) using ARPES. With the increasing of Cu dopant from $x = 0.019$ to $x = 0.14$, the Fermi level increases gradually in a fashion of electron doping, while the overall band dispersions remain basically the same, which is similar to a rigid-band-like model but with a carrier doping evidently less than expected from a rigid-band model. With increasing Cu dopant, the near-E_F spectral weight reduces and the localized Cu 3*d* states grow up at high binding energies. The potential correlation between the superconductivity and the change of electronic structures is also discussed.

We gratefully acknowledge the experimental support by Dr. M. Shi, N. C. Plumb, and N. Xu at the SLS. This work was supported by National Natural Science Foundation of China (Grants No. 11190022, No. 11190021, No. 11179036), the National Basic Research Program of China (973 Program, Grants No. 2012CB922002, No. 2012CB922004), the Chinese Academy of Sciences, the Strategic Priority Research Program (B) (Grant No. XDB04040100). Z.S. acknowledges the support by the Fundamental Research Funds for the Central Universities.

*zsun@ustc.edu.cn

[1] Y. Kamihara, T. Watanabe, M. Hirano, and H. Hosono, J. Am. Chem. Soc. **130**, 3296 (2008).
[2] X. H. Chen, T. Wu, G. Wu, R. H. Liu, H. Chen, and D. F. Fang, Nature (London) **453**, 761-762 (2008).
[3] M. Rotter, M. Tegel, and D. Johrendt, Phys. Rev. Lett. **101**, 107006 (2008).
[4] P. C. Canfield, S. L. Budko, N. Ni, J. Q. Yan, and A. Kracher, Phys. Rev. B **80**, 060501(R) (2009).
[5] S. Jiang, H. Xing, G. F. Xuan, C. Wang, Z. Ren, C. M. Feng, J. H. Dai, Z. A. Xu, and G. H. Cao, J. Phys.: Condens. Matter **21**, 382203 (2009).
[6] W. Schnelle, A. Leithe-Jasper, R. Gumeniuk, U. Burkhardt, D. Kasinathan, and H. Rosner, Phys. Rev. B **79**, 214516 (2009).
[7] N. Xu, T. Qian, P. Richard, Y. B. Shi, X. P. Wang, P. Zhang, Y. B. Huang, Y. M. Xu, H. Miao, G. Xu, G. F. Xuan, W. H. Jiao, Z. A. Xu, G. H. Cao, and H. Ding, Phys. Rev. B **86**, 064505 (2012).
[8] V. Brouet, F. Rullier-Albenque, M. Marsi, B. Mansart, M. Aichhorn, S. Biermann, J. Faure, L. Perfetti, A. Taleb-Ibrahimi, P. Le Fevre, F. Bertran, A. Forget, and D. Colson, Phys. Rev. Lett. **105**, 087001 (2010).
[9] R. S. Dhaka, C. Liu, R. M. Fernandes, R. Jiang, C. P. Strehlow, T. Kondo, A. Thaler, J. Schmalian, S. L. Bud'ko, P. C. Canfield, and A. Kaminski, Phys. Rev. Lett. **107**, 267002 (2011).
[10] C. Liu, T. Kondo, R. M. Fernandes, A. D. Palczewski, E. D. Mun, N. Ni, A. N. Thaler, A. Bostwick, E. Rotenberg, J. Schmalian, S. L. Bud'ko, P. C. Canfield, and A. Kaminski, Nat. Phys. **6**, 419 (2010).
[11] C. Liu, A. D. Palczewski, R. S. Dhaka, T. Kondo, R. M. Fernandes, E. D. Mun, H. Hodovanets, A. N. Thaler, J. Schmalian, S. L. Bud'ko, P. C. Canfield, and A. Kaminski, Phys. Rev. B **84**, 020509 (2011).
[12] H. Wadati, I. Elfimov, and G. A. Sawatzky, Phys. Rev. Lett. **105**, 157004 (2010).
[13] S. Ideta, T. Yoshida, M. Nakajima, W. Malaeb, T. Shimojima, K. Ishizaka, A. Fujimori, H. Kimigashira, K. Ono, K. Kihou, Y. Tomioka, C. H. Lee, A. Iyo, H. Eisaki, T. Ito, and S. Uchida, Phys. Rev. B **87**, 201110(R) (2013).
[14] J. Li, Y. F. Guo, S. B. Zhang, S. Yu, Y. Tsujimoto, H. Kontani, K. Yamaura, and E. Takayama-Muromachi, Phys. Rev. B **84**, 020513(R) (2011).
[15] J. Li, Y. F. Guo, S. B. Zhang, J. Yuan, Y. Tsujimoto, X. Wang, C. I. Sathish, Y. Sun, S. Yu, W. Yi, K. Yamaura, E. Takayama-Muromachiu, Y. Shirako, M. Akaogi, and H. Kontani, Phys. Rev. B **85**, 214509 (2012).
[16] N. Ni, A. Thaler, J. Q. Yan, A. Kracher, E. Colombier, S. L. Bud'ko, P. C. Canfield, and S. T. Hannahs, Phys. Rev. B **82**, 024519 (2010).
[17] P. C. Canfield and S. L. Bud'ko, Annu. Rev. Condens. Matter Phys. **1**, 27 (2010).
[18] Y. J. Yan, P. Cheng, J. J. Ying, X. G. Luo, F. Chen, H. Y. Zou, A. F. Wang, G. J. Ye, Z. J. Xiang, J. Q. Ma, and X. H. Chen, Phys. Rev. B **87**, 075105 (2013).
[19] S. Ideta, T. Yoshida, I. Nishi, A. Fujimori, Y. Kotani, K. Ono, Y. Nakashima, S. Yamaichi, T. Sasagawa, M. Nakajima, K. Kihou, Y. Tomioka, C. H. Lee, A. Iyo, H. Eisaki, T. Ito, S. Uchida, and R. Arita, Phys. Rev. Lett. **110**, 107007 (2013).
[20] P. Cheng, B. Shen, F. Han, and H. H. Wen, arXiv:1304.4568.
[21] J. A. McLeod, A. Buling, R. J. Green, T. D. Boyko, N. A. Skorikov, E. Z. Kurmaev, M. Neumann, L. D. Finkelstein, N. Ni, and A. Thaler, J. Phys.: Condens. Matter **24**, 215501 (2012); D. J. Singh, Phys. Rev. B **79**, 153102 (2009).
[22] D. J. Singh, Phys. Rev. B **79**, 153102 (2009).
[23] A. F. Wang, X. G. Luo, Y. J. Yan, J. J. Ying, Z. J. Xiang, G. J. Ye, P. Cheng, Z. Y. Li, W. J. Hu, and X. H. Chen, Phys. Rev. B **85**, 224521 (2012).

[24] A. F. Wang, J. J. Lin, P. Cheng, G. J. Ye, F. Chen, J. Q. Ma, X. F. Lu, B. Lei, X. G. Luo, and X. H. Chen, Phys. Rev. B **88**, 094516 (2013).

[25] Y. Zhang, C. He, Z. R. Ye, J. Jiang, F. Chen, M. Xu, Q. Q. Ge, B. P. Xie, J. Wei, M. Aeschlimann, X. Y. Cui, M. Shi, J. P. Hu, and D. L. Feng, Phys. Rev. B **85**, 085121 (2012).

[26] S. T. Cui, S. Y. Zhu, A. F. Wang, S. Kong, S. L. Ju, X. G. Luo, X. H. Chen, G. B. Zhang, and Z. Sun, Phys. Rev. B **86**, 155143 (2012).

[27] K. Kusakabe and A. Nakanishi, J. Phys. Soc. Jpn. **78**, 124712 (2009).

[28] S. Q. Deng, J. Kohler, and A. Simon, Phys. Rev. B **80**, 214508 (2009).

[29] Y. Zhang, L. X. Yang, M. Xu, Z. R. Ye, F. Chen, C. He, H. C. Xu, J. Jiang, B. P. Xie, J. J. Ying, X. F. Wang, X. H. Chen, J. P. Hu, M. Matsunami, S. Kimura, and D. L. Feng, Nature Mater. **10**, 273 (2011).

[30] Z. H. Liu, P. Richard, K. Nakayama, G. F. Chen, S. Dong, J. B. He, D. M. Wang, T. L. Xia, K. Umezawa, T. Kawahara, S. Souma, T. Sato, T. Takahashi, T. Qian, Y. B. Huang, N. Xu, Y. B. Shi, H. Ding, and S. C. Wang, Phys. Rev. B **84**, 064519 (2011).

[31] T. Berlijn, C. H. Lin, W. Garber, and W. Ku, Phys. Rev. Lett. **108**, 207003 (2012).

[32] K. Nakamura, R. Arita, and H. Ikeda, Phys. Rev. B **83**, 144512 (2011).

[33] D. Innocenti, S. Caprara, N. Poccia, A. Ricci, A. Valletta, and A. Bianconi, Supercond. Sci. Technol. **24**, 015012 (2011).